Journal of Physics: Conference Series **194** (2009) 012055 doi:10.1088/1742-6596/194/1/012055

Time-resolved IR laser-assisted XUV photoelectron spectroscopy of metal surfaces

C.-H. Zhang and U. Thumm

Department of Physics, Kansas State University, Manhattan, Kansas 66506, USA

E-mail: thumm@phys.ksu.edu

Abstract. Photoemission of localized and delocalized electrons from an (adsorbate-covered) metal surface by an XUV pulse of length τ_X into the field of a delayed IR laser pulse with carrier period T_L allows for the time-resolved observation of surface and adsorbate electronic processes. For $\tau_X \ll T_L$, the energy of the emitted photoelectrons (PEs) oscillates with period T_L as a function of the XUV-IR pulse delay, leading to streaked PE spectra. In contrast, for $\tau_X \gtrapprox T_L$, the PE spectrum is characterized by a satellite structure of sideband peaks located at integer multiples of the IR photon energy from the main photoemission peak. We present a theoretical model that allows us to discuss both, streaked and sideband photoemission spectra in comparison with recent experiments.

1. Introduction

State-of-the-art ultra-fast laser technology [1, 2, 3, 4, 5] enables the resolution at a timescale of the order of 100 attoseconds (1 as=10^{-18} s) of the laser-induced electronic dynamics in atoms [6, 7, 8, 9] and molecules [10, 11, 12]. The recent successful extension of time-resolved laser-assisted PE spectroscopy to solid surfaces [13, 14, 15, 16] promises the time-resolved observation of electronic processes in condensed matter systems that may involve a single active electron [14, 17], the correlated dynamics of two electrons [6, 15], or collective electronic excitations [18, 19, 20] (Fig. 1). Such time-resolved investigations at the intrinsic time-scale of the active electron(s) or collective modes will provide information about the structure and dynamics of delocalized valence and conduction band states, electron transport in solids, and the decay of collective excitations near solid surfaces, e.g., of novel plasmonic devices [19, 21].

2. Theory

2.1. Direct photoemission for localized and delocalized states

We describe the absorption of a single XUV photon, resulting in the emission of an electron from an initial Bloch state $\Psi_{\mathbf{k}_i}(\mathbf{r},t) = \Psi_{\mathbf{k}_i}(\mathbf{r})e^{-i\varepsilon_{\mathbf{k}_i}t}$ (with crystal momentum $\mathbf{k}_i$ and energy $\varepsilon_{\mathbf{k}_i}$) of a metal surface (or adsorbate) to an IR field-dressed final continuum state $\Psi_f(\mathbf{r},t)$, in terms of the transition amplitude

$$T_{\mathbf{k}_f,\mathbf{k}_i}(\tau) = -i\int dt\langle\Psi_f(\mathbf{r},t)|zE_X(t+\tau)|\Psi_{\mathbf{k}_i}(\mathbf{r},t)\rangle, \tag{1}$$

where τ is the time delay between the IR and XUV pulses. In this expression, the dipole-length gauge is applied for the perturbative interaction of the PE with the XUV electric field $\mathbf{E}_X(t)$,

© 2009 IOP Publishing Ltd

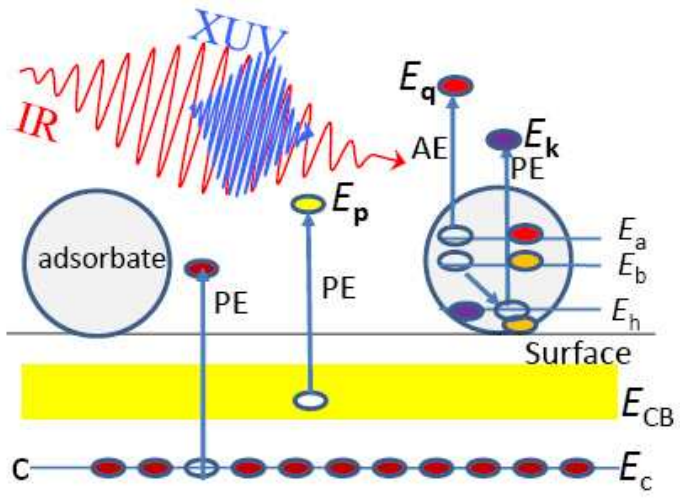

Figure 1. (Color online) Sketch of the emission of substrate (core level and conduction band) and adsorbate (core level and Auger) electrons by an XUV pulse. Photoreleased electrons are exposed to a weak delayed IR pulse.

while the interaction of the released PE with the IR field $\mathbf{E}_L(t)$ is taken into account in strong-field approximation [17, 22, 23] by representing the final state $\Psi_f(\mathbf{r},t)$ as a damped Volkov wave function

$$\Psi_{\mathbf{k}_f}(\mathbf{r},t) = \Psi^V_{\mathbf{k}_f}(\mathbf{r},t)\left[\Theta(z) + e^{\kappa z}\Theta(-z)\right]. \tag{2}$$

$\Theta(z)$ is the unit step function, and $\Psi^V_{\mathbf{k}_f}(\mathbf{r},t)$ is the usual Volkov wavefunction

$$\Psi^V_{\mathbf{k}_f}(\mathbf{r},t) = \frac{1}{(2\pi)^{3/2}} e^{i[\mathbf{k}_f + \mathbf{A}_L(t)]\cdot\mathbf{r}} e^{i\phi_{\mathbf{k}_f}(t) - i\varepsilon_{\mathbf{k}_f} t} \tag{3}$$

with momentum $\mathbf{k}_f$, energy $\varepsilon_{\mathbf{k}_f} = \mathbf{k}_f^2/2$, phase $\phi_{\mathbf{k}_f} = \frac{1}{2}\int_t^\infty dt_1 \left[2\mathbf{k}_f \cdot \mathbf{A}_L(t_1) + \mathbf{A}_L^2(t_1)\right]$, and vector potential $\mathbf{A}_L(t) = \int_t^\infty dt_1 \mathbf{E}_L(t_1)$. In the numerical applications discussed below, we assume grazingly incident laser pulses that are linearly polarized perpendicular to the surface and electron emission normal to the surface. Unless stated otherwise, we use atomic units with $\hbar$, electron mass, elementary charge, and Bohr radius all being equal to 1.

The damping factor $e^{\kappa z}$ in (2) accounts for the finite mean-free path $\lambda = 1/2\kappa$, i.e., for the electronic transport, of PEs inside the solid [24, 25]. Integration of (1) over all momenta $\mathbf{k}_i$ inside the first Brillouin zone (for the case of photoemission from substrate or adsorbate core levels (CLs)) or over the Fermi volume (for emission from delocalized conduction band (CB) states), yields the photoemission probability

$$P(\mathbf{k}_f,\tau) = \int d\mathbf{k}_i \left|T_{\mathbf{k}_f,\mathbf{k}_i}(\tau)\right|^2. \tag{4}$$

The initial state $\Psi_{\mathbf{k}_i}$ is composed of Bloch waves, $\Psi^-_{\mathbf{k}_i}$ and $\Psi^+_{\mathbf{k}_i}$ for the motion of an electron inside the solid towards and away from the surface with crystal momenta $\mathbf{k}_i^\pm = (\mathbf{k}_{i,\parallel}, \pm k_{i,z})$, respectively, and a transmitted part that decays exponentially into the vacuum ($z > 0$) and is negligible in the applications discussed below.

For photoemission from delocalized states, we represent the substrate CB in jellium approximation, which models the surface in terms of the step potential [26] $U(\mathbf{r}) = -U_0\Theta(-z)$, with $U_0 = \varepsilon_F + W$, Fermi energy ε_F, and the work function W, such that the initial CB wave functions are [27]

$$\Psi^{CB}_{\mathbf{k_i}}(\mathbf{r},t) = \frac{e^{-i\varepsilon_{\mathbf{k}_i}t}}{(2\pi)^{3/2}} e^{i\mathbf{k}_{i,\parallel}\cdot\mathbf{r}_\parallel}\left(e^{ik_{i,z}z} + Re^{-ik_{i,z}z}\right), \tag{5}$$

with $\varepsilon_{\mathbf{k}_i} = \mathbf{k}_i^2/2 - U_0$, $R = (k_{i,z} - i\gamma)/(k_{i,z} + i\gamma)$, $\gamma = \sqrt{2U_0 - k_{i,z}^2}$.

For photoemission from localized CLs, we construct a tight-binding initial wave function by superimposing atomic orbitals ψ_c with binding energy ε_B that are centered at the lattice points $\{\mathbf{R}_j\}$ of the substrate,

$$\Psi_{\mathbf{k}_i}^{\pm}(\mathbf{r}, t) = \sum_j e^{i\mathbf{k}_i^{\pm}\cdot\mathbf{R}_j} \psi_c(\mathbf{r} - \mathbf{R}_j) e^{-i\varepsilon_B t}. \tag{6}$$

Thus, the corresponding transition amplitude includes interlayer interference effects in terms of a coherent sum over contributions to the photocurrent from substrate layers (with spacing a) located within a distance $\approx \lambda$ from the surface. In our numerical applications below, we model $\psi_c(\mathbf{r})$ by adjusting hydrogenic ground state orbitals to the CL binding energy.

2.2. Photoemission followed by Auger relaxation

The coherent quantum mechanical modeling of XUV photoemission and subsequent relaxation by the emission of Auger electrons (AEs) from substrate or adsorbate CLs involves three bound and two continuum single-particle states, given by the core-hole level Ψ_h, two excited levels Ψ_a and Ψ_b, and the continuum states of the emitted PE and AE, $\Psi_{\mathbf{k}}$ and $\Psi_{\mathbf{q}}$, respectively. The bound single-particle states Ψ_i, $i = h,\ a,\ b$, are eigenstates of the atomic Hamiltonian H_{at} with binding energies ε_i. Neglecting Coulomb interactions, the continuum states $\Psi_{\mathbf{s}}$ with momenta $\mathbf{s} = \mathbf{k},\ \mathbf{q}$ can be approximated in strong field approximation as Volkov states with energies $\varepsilon_{\mathbf{s}}$.

We describe the adsorbate-CL-ionization-followed-by Auger-relaxation process [15] in terms of anti-symmetrized products of single-particle states for the ground state, $|\Psi_h, \Psi_a, \Psi_b\rangle$, CL-photoemission, $|\Psi_{\mathbf{k}}, \Psi_a, \Psi_b\rangle$, and the final channel after relaxation of the adsorbate $|\Psi_{\mathbf{k}}, \Psi_h, \Psi_{\mathbf{q}}\rangle$. Following [28], we expand the total two-electron state in these three channels,

$$|\Phi(t)\rangle = |\Psi_h, \Psi_a, \Psi_b\rangle + \int d\mathbf{k}\, b_{\mathbf{k}}(t) |\Psi_{\mathbf{k}}, \Psi_a, \Psi_b\rangle + \int d\mathbf{k} d\mathbf{q}\, c_{\mathbf{k},\mathbf{q}}(t) |\Psi_{\mathbf{k}}, \Psi_h, \Psi_{\mathbf{q}}\rangle, \tag{7}$$

assuming sufficiently weak laser intensities for depletion of the initial channel to be irrelevant.

The coefficients $b_{\mathbf{k}}(t)$ and $c_{\mathbf{k},\mathbf{q}}(t)$ are determined by inserting (7) into the time-dependent Schrödinger equation with the Hamiltonian

$$\hat{H}(t) = \sum_i H_{at}(i) + \frac{1}{2}\sum_{i\neq j} V(\mathbf{r}_i - \mathbf{r}_j) + \sum_i \left[\mathbf{E}_L(t) + \mathbf{E}_X(t+\tau)\right]\cdot\mathbf{r}_i, \tag{8}$$

with the Coulomb potential $V(\mathbf{r}_i - \mathbf{r}_j)$ between electrons i and j. Neglecting Coulomb-pair interactions between single-particle states, except for the interaction $V_{\mathbf{q}} = \langle\psi_a\psi_b|V|\psi_h\psi_{\mathbf{q}}\rangle$ between ψ_a and ψ_b that drives the Auger-decay, and using $\Psi_i(\mathbf{r}, t) = \psi_i(\mathbf{r}) e^{-i\varepsilon_i t}$, $i = h,\ a,\ b,\ \mathbf{k},\ \mathbf{q}$, results in the coupled equations

$$i\partial_t b_{\mathbf{k}}(t) = \mathbf{E}_X(t+\tau)\cdot\mathbf{d}_{h,\mathbf{p}}^{CL} e^{i(\varepsilon_{\mathbf{k}}+\varepsilon_h)t - i\phi_{\mathbf{k}}(t)} + \int d\mathbf{q}\, V_{\mathbf{q}}\, c_{\mathbf{k},\mathbf{q}}(t) e^{i(W_A - \varepsilon_{\mathbf{q}})t + i\phi_{\mathbf{q}}(t)}, \tag{9}$$

$$i\partial_t c_{\mathbf{k},\mathbf{q}}(t) = V_{\mathbf{q}}^*\, b_{\mathbf{k}}(t) e^{-i(W_A - \varepsilon_{\mathbf{q}})t - i\phi_{\mathbf{q}}(t)}, \tag{10}$$

with $W_A = \varepsilon_a + \varepsilon_b - \varepsilon_h$ and the dipole matrix element between ψ_h and the damped final Volkov state (2) with canonical momentum $\mathbf{p} = \mathbf{k} + \mathbf{A}_L(t)$

$$d_{h,\mathbf{p}}^{CL} = \frac{1}{(2\pi)^{3/2}} \int d\mathbf{r}\, e^{i\mathbf{p}\cdot\mathbf{r}} \left[\Theta(z) + e^{\kappa z}\Theta(-z)\right] z\psi_h(\mathbf{r}). \tag{11}$$

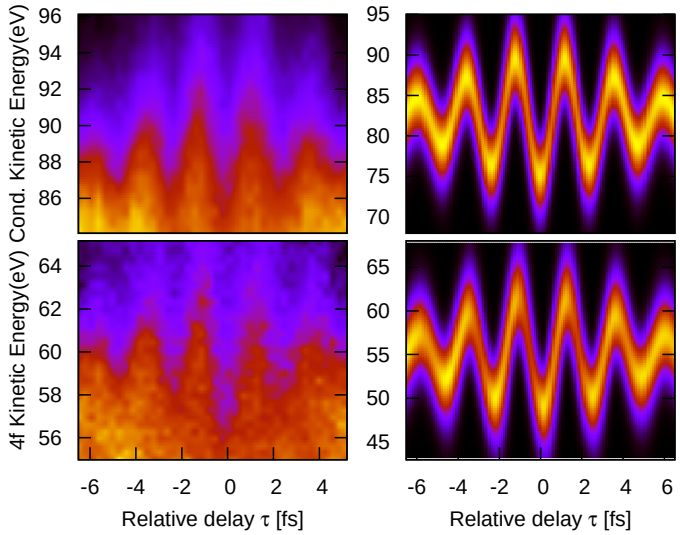

Figure 2. (Color online) Time-resolved PE spectra for emission from the CB (top) and $4f$-CLs (bottom) of a W(110) surface as a function of the delay between the XUV and IR pulses for decadic color scales. Experimental results of [14] (left) in comparison with our calculation (right).

By integrating (10), inserting the result into (9), and integrating (9), we find the probability $P^{PE+AE}(\mathbf{k},\mathbf{q},\tau) = |c(\mathbf{k},\mathbf{q},t\to\infty)|^2$ for the coherent emission of PEs and AEs with momenta $\mathbf{k}$ and $\mathbf{q}$,

$$P^{PE+AE}(\mathbf{k},\mathbf{q},\tau) = \left| \int_{-\infty}^{+\infty} dt V_{\mathbf{q}}^{*} e^{i(\varepsilon_{\mathbf{q}}-W_A)t - i\phi_{\mathbf{q}}(t)} \int_{-\infty}^{t} dt' e^{\frac{\Gamma}{2}(t'-t)} e^{i(\varepsilon_h+\varepsilon_{\mathbf{k}})t' - i\phi_{\mathbf{k}}(t')} \mathbf{E}_X(t'+\tau)\cdot \mathbf{d}_{h,\mathbf{p}}^{CL} \right|^2 . \tag{12}$$

In order to arrive at (12), we applied a "weak-memory" (or Markov) approximation for $b_{\mathbf{k}}(t)$ and neglected the energy shift $\Delta = -\mathrm{P}\int d\mathbf{q} \frac{|V_{\mathbf{q}}|^2}{\varepsilon_{\mathbf{q}}-W_A}$ of the PEs due to electronic correlation [29]. In our numerical applications below, we will treat the core-hole decay rate $\Gamma = 2\pi \int d\mathbf{q} |V_{\mathbf{q}}|^2 \delta(\varepsilon_{\mathbf{q}} - W_A)$ as an adjustable parameter.

3. Numerical results and comparison with experiments

3.1. Attosecond time-resolved photoemission streaking spectra

The basic setup of a time-resolved photoemission experiment on a metal surface is illustrated in Fig. 1. In order to obtain streaked PE spectra, the XUV pulse length is required to be short on the time scale of the IR laser period, $\tau_X \ll T_L$. An as extreme XUV light pulse is used to release electrons from either bound core levels or delocalized CB states. The released PEs get exposed to (and "streaked by") by the same IR probe pulse that was used to generate the XUV pulse via harmonic generation [30]. The two laser pulses are thus synchronized with a precisely adjustable time delay τ. By varying τ the time-resolved PE kinetic energy distribution $P(E,\tau)$ can be recorded. By applying this technique, Cavalieri *et al.* [14] measured a relative delay of 110 ± 70 as between the detection of PEs that are emitted by absorption of a single XUV photon from $4f$-core and CB levels.

To compare our model calculations with this streaking experiment, we assume IR and XUV pulses with Gaussian envelopes,

$$E_{L(X)}(t) = E_{L(X)0}(t)\cos(\omega_{L(X)}t), \quad E_{L(X)0}(t) = E_{L(X)0}\, e^{-2\ln 2\left(t/\tau_{L(X)}\right)^2}, \tag{13}$$

respectively, and use experimental parameters [14] for pulse lengths ($\tau_L = 6.5$ fs and $\tau_X = 0.29$ fs (FWHM)), photon energies ($\hbar\omega_L = 1.7$ eV and $\hbar\omega_X = 91$ eV), and IR peak intensity

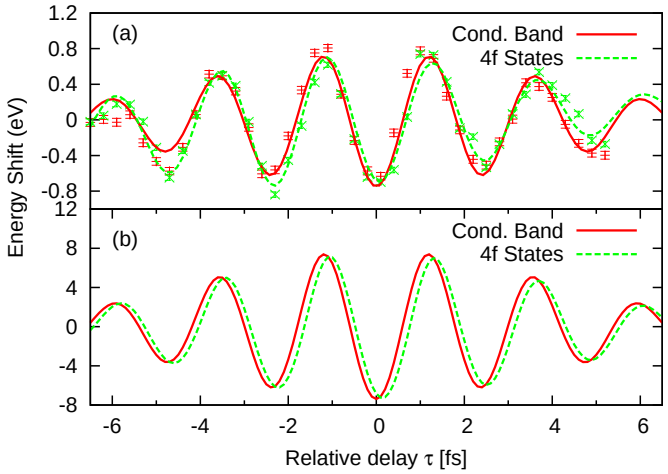

Figure 3. (Color online) Streaked electron spectra for photoemission from CB and $4f$-CLs of a W(110) surface: $\bar{E}$ [31] as a function of τ. (a) Experimental results [14]. The damped sinusoidal curves are fits to the raw experimental data (points with error bars). (b) Calculated results showing a relative shift of $\Delta\tau = 110$ as between the two groups of electrons. The COEs for the $4f$-PEs are multiplied by 2.5 in (a) and 1.1 in (b).

($I_L = 2 \times 10^{12}$ W/cm^2). For the W(110) surface we use measured values for the work function ($W = 5.5$ eV), Fermi energy ($\varepsilon_F = 4.5$ eV), and the lattice constant in the direction perpendicular to the surface ($a = 3.13$ Å).

We calculated energy-resolved spectra $P_{cb}(E,\tau)$ and $P_{4f}(E,\tau)$ for the two groups of PEs as a function of τ. The comparison of experiment and theory in Fig. 2 shows that the simulated IR pulse modulation of the PE kinetic energy agrees with the experiment. In order to find the temporal shift between the two calculated spectra in the right column of Fig. 2, we determined their center-of-energies (COEs) in Fig. 3 [31]. The temporal shift $\Delta\tau$ between $4f$ CL and CB electrons is extracted from Fig. 3. We found that the measured value of $\Delta\tau = 110$ as can be obtained by adjusting the electron-mean free path to $\lambda = 2.65$ Å. It can be shown that nonzero values for $\Delta\tau$ requires (i) interference between electrons that are photoemitted from $4f$-core levels from different layers in the solid, and (ii) a finite mean free path of the PEs inside the solid [23].

3.2. Laser-assisted photoemission from adsorbate-covered metal surfaces

In a recent roof-of-principle experiment [15] on Xe-covered Pt(111) surfaces and overlapping synchronized XUV and IR pulses, PEs electrons that are emitted after absorption of a single XUV photon from localized CLs and delocalized CB states were recorded (Fig. 1). By investigating the relative peak heights of the main peak and first sidebands in the PE spectrum as a function of the XUV-IR delay τ, the decay lifetime of Xe adsorbate core-hole states could be extracted. In this setup, the XUV pulse length is required to be comparable to or longer than the IR laser period, $\tau_X \gtrsim T_L$.

Our model calculation reproduces the measured [15] sideband structures. Compared to PE emission from gaseous atoms, we find that sideband intensities in PE spectra from substrate core-levels are enhanced due to interfering photoemission from different layers in the substrate, indicating that the sideband intensity encodes information on the transport of PEs in the solid. We employ IR and XUV laser electric field pulses (13) with parameters from the experiment [15] for pulse lengths (FWHM) ($\tau_L = 35.5$ fs, $\tau_X = 5.5$ fs) and photon frequencies ($\omega_L = 1.6$ eV/$\hbar$, $\omega_X = 91$ eV/$\hbar$). With a peak intensity $I_L = 7\times10^{10}$ W/cm^2 of about 1/2 of the experimental IR peak intensity, we take into account the effect of variable peak intensities inside the experimental focal volume.

The left column of Fig. 4 shows our numerical results for $P^{PE(AE)}(E)$ in comparison with the experiment [15] at $\tau = 0$. For direct photoemission from the Pt CB (top left graph), the

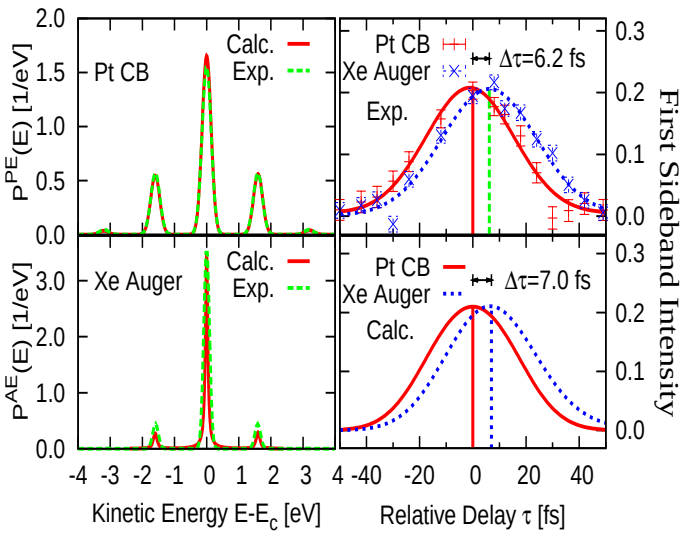

Figure 4. (Color online) Theoretical and experimental [15] PE spectra for laser-assisted photoemission from a Xe/Pt(111) surface. **Left:** Sideband intensities for no delay ($\tau = 0$) between XUV and IR pulses for XUV-emitted Pt CB electrons from the Fermi level (top) and Xe AEs (bottom). **Right:** Experimental (top) and calculated (bottom) first sideband intensities for Pt CB electrons and Xe AEs as a function of τ, revealing a temporal shift $\Delta\tau$. Sideband intensities in the AE spectra are multiplied by 2.16.

line profiles assumed in [15] have the same functional (Gaussian) form

$$P_n^{PE}(E) \sim e^{-(E-W_A+n\hbar\omega_L)^2/2(\sigma_n^{PE})^2} \tag{14}$$

predicted by our model [29], and the calculated widths $\sigma_1^{PE} = 0.140$ eV and $\tau_1^{PE} = 39$ fs agree with the experimental values 0.142 eV and 39 fs, respectively. For the energy dependence in the Xe *NOO* Auger spectra, the analysis in [15] is based on a Gaussian line profile. In contrast, our model can be shown analytically [29] to lead to the Lorentzian profile

$$P_n^{AE}(E) \sim \frac{\sigma_n^{AE}/2}{(E - W_A + n\hbar\omega_L)^2 + (\sigma_n^{AE}/2)^2}. \tag{15}$$

Irrespective of this difference in the Auger-line profiles, by adjusting $\Gamma = 0.14$ fs^{-1} the calculated first sideband intensities $I^{AE}_{+1(-1)}(0) = 0.099$ (0.105) agree well with the corresponding experimental results 0.094 (0.102). The graphs on the right of Fig. 4 show experimental (top right graph) and corresponding calculated (bottom right graph) first sideband intensities as a function of τ. The calculated temporal shift $\Delta\tau = 7$ fs between the Pt CB and the Xe AEs agrees well with the experimental value of 6.2 fs.

We modeled the influence of the solid environment on the transport of photoreleased electrons solely in terms of a heuristic damping factor that includes the mean free path λ. Even though this approximation neglects details of electron scattering and diffraction effects, it demonstrates that sideband intensities can be used to explore transport properties of core-level PEs inside a solid (Fig. 5): the coherent photoemission from periodically spaced CLs causes a λ-dependent redistribution of emission probability between the main peak and sidebands relative to photoemission from isolated atoms. For $\lambda < 0.1$ the relative sideband peak heights are equal to the corresponding atomic (gas phase) case. However, as λ increases, the main peak gets depleted while the sidebands become enhanced. This enhancement can be traced analytically [29], and the n-th sideband amplitude in (4) for photoemission from CLs is proportional to

$$e^{in\omega_L t} \sum_{l+m=n} J_l\left(\frac{kE_{L0}(t)}{\omega_L^2}\right) J_m\left(\frac{E_{L0}(t)a}{\omega_L}\right). \tag{16}$$

Note that the argument of the Bessel function J_m depends on the interlayer spacing a and that both l and m combine to a given sideband order n. For $n \neq 0$, all terms have the same sign, such that the sideband intensities interfere constructively.

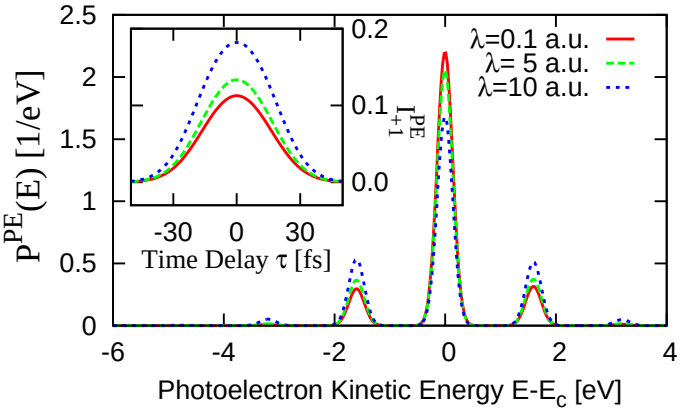

Figure 5. ((Color online) Sideband enhancement in the PE spectrum of the $5p_{3/2}$ band in Pt. The main peak is centered at E_c = 39.3 eV. **Inset:** First sideband intensity $I^{PE}_{+1}(\tau)$.

4. Conclusions

The finite mean free path and interfering photoemission from periodically spaced CLs lead to the observed temporal shift in the streaked PE spectra between CL and CB PEs. Our numerical results reproduce both measured relative temporal shifts in streaked PE spectra and observed streaking amplitudes [14].

Comparing the profiles of sideband peaks in XUV photoemission from localized atomic and delocalized metal CB levels with the spectrum of AEs emitted during the decay of an adsorbate core hole, we analyzed the relative delay of substrate PEs and adsorbate AEs in agreement with a recent experiment [15]. We also investigated sideband profiles in PE and AE spectra, mostly in support of a previous analysis of measured PE spectra [15]. In addition, we found an intensity redistribution between the main and sideband peaks in core level PE spectra from metals surfaces that is related to the transport of photoreleased electrons in the substrate. Since the transport (included in our model through the mean-free path, λ) depends on the PE kinetic energy, and thus on ω_X, we anticipate future tests of this predicted sideband enhancement effect in experiments with tunable XUV wavelength.

Acknowledgments

This work was supported by the NSF and the Division of Chemical Sciences, Office of Basic Energy Sciences, Office of Energy Research, US DOE.

References

[1] Hentschel M, Kienberger R, Spielmann C, Reider G A, Milosevic N, Brabec T, Corkum P, Heinzmann U, Drescher M and Krausz F 2001 *Nature* **414** 509
[2] Paul P M, Toma E S, Breger P, Mullot G, Augë F, Balcou P, Muller H G and Agostini P 2001 *Science* **292** 1689
[3] Sansone G, Benedetti E, Calegari F, Vozzi C, Avaldi L, Flammini R, Poletto L, Villoresi P, Altucci C, Velotta R, Stagira S, De Silvestri S and Nisoli M 2006 *Science* **314** 443
[4] Corkum P B and Krausz F 2007 *Nature Phys.* **3** 381
[5] Goulielmakis E , Schultze M, Hofstetter M, Yakovlev V S, Gagnon J, Uiberacker M, Aquila A L, Gullikson E M, Attwood D T, Kienberger R, Krausz F and Kleineberg U 2008 *Science* **320** 1614
[6] Drescher M, Hentschel M, Kienberger R, Uiberacker M, Yakovlev V, Scrinzi A, Westerwalbesloh T, Kleineberg U, Heinzmann U and Krausz F 2002 *Nature* **419** 803
[7] Kienberger R, Goulielmakis E, Uiberacker M, Baltuska A, Yakovlev V, Bammer F, Scrinzi A, Westerwalbesloh T, Kleineberg U, Heinzmann U, Drescher M and Krausz F 2004 *Nature* **427** 817
[8] Uiberacker M , Uphues T, Schultze M, Verhoef A J, Yakovlev V, Kling M F, Rauschenberger J, Kabachnik N N, Schöder H, Lezius M, Kompa K L, Muller H G, Vrakking M J J, Hendel S, Kleineberg U, Heinzmann U, Drescher M and Krausz F 2007 *Nature* **446** 627
[9] Johnsson P, Mauritsson J, Remetter T, LHuillier A and Schafer K J 2007 *Phys. Rev. Lett.* **99** 233001

[10] Niikura H, Légaré F, Hasbani R, Ivanov M Y, Villeneuve D M and Corkum P B 2003 *Nature* **421** 826
[11] Kling M F , Siedschlag C, Verhoef A J, Khan J I, Schultze M, Uphues T, Ni Y, Uiberacker M, Drescher M, Krausz F and Vrakking M J J 2006 *Science* **312** 246
[12] Staudte A, Pavicic D, Chelkowski S, Zeidler D, Meckel M, Niikura H, Schöffler M, Schössler S, Ulrich B, Rajeev P P, Weber T, Jahnke T, Villeneuve D M, Bandrauk A D, Cocke C L, Corkum P B and Dörner R 2007 *Phys. Rev. Lett.* **98** 073003
[13] Miaja-Avila L, Lei C, Aeschlimann M, Gland J L, Murnane M M, Kapteyn H C and Saathoff G 2006 *Phys. Rev. Lett.* **97** 113604
[14] Cavalieri A L, Müller N, Uphues T, Yakovlev V S, Baltus caronka A, Horvath B, Schmidt B, Blümel L, Holzwarth R, Hendel S, Drescher M, Kleineberg U, Echenique P M, Kienberger R, Krausz F and Heinzmann U 2007 *Nature* **449** 1029
[15] Miaja-Avila L, Saathoff G, Mathias S, Yin J, La-o-vorakiat C, Bauer M, Aeschlimann M, Murnane M M and Kapteyn H C 2008 *Phys. Rev. Lett.* **101** 046101
[16] Saathoff G, Miaja-Avila L, Aeschlimann M, Murnane M M and Kapteyn H C 2008 *Phys. Rev. A.* **77** 022903
[17] Baggesen J C and Madsen L B 2008 *Phys. Rev. A*, **78** 032903
[18] Kubo A, Onda K, Petek H, Sun Z, Jung Y S and Kim H K 2005 *Nano Lett.* **5** 1123
[19] Sukharev M and Seideman T 2006 *Nano Lett.* **6** 1123
[20] Stockman M I, Kling M F, Kleineberg U and Krausz F 2007 *Nature Phot.* **1** 539
[21] Le F, Lwin N Z, Halas N J and Nordlander P 2007 *Phys. Rev. B* **76** 165410
[22] Kitzler M, Milosevic N, Scrinzi A, Krausz F and Brabec T 2002 *Phys. Rev. Lett.* **88** 173904
[23] Zhang C H and Thumm U 2009 *Phys. Rev. Lett.* 102 123601
[24] Hüfner S 2003 *Photoelectron Spectroscopy* (Berlin: Springer)
[25] Feibelman P J 1974 *Phys. Rev. B* **10** 4932
[26] Zangwill A 1988 *Physics at surfaces* (New York: Cambridge University Press)
[27] Thumm U 1992 *J. Phys. B* **25** 421
[28] Smirnova O, Yakovlev V S and Scrinzi A 2003 *Phys. Rev. Lett.* **91** 253001
[29] Zhang C H and Thumm U 2009 *Phys. Rev. A* **80** 032902
[30] Corkum P B 1993 *Phys. Rev. Lett.* **71** 1994
[31] The COE of the spectrum is defined as $\bar{E}(\tau) = \int_{E_{min}}^{E_{max}} dEEP(E,\tau) / \int_{E_{min}}^{E_{max}} dEP(E,\tau) - E_c$. E_c is the spectral peak position without the IR field. $E_{min} = 47$ (66) and $E_{max} = 66(110)$ eV for $4f$ (CB) PEs, respectively.